Published in final edited form as:

Nanotoxicology. 2015 ; 9(6): 769–779. doi:10.3109/17435390.2014.976603.

Small Airway Epithelial Cells Exposure to Printer-Emitted Engineered Nanoparticles Induces Cellular Effects on Human Microvascular Endothelial Cells in an Alveolar-Capillary Co-Culture Model

Jennifer D. Sisler[1], **Sandra V. Pirela**[2], **Sherri Friend**[1], **Mariana Farcas**[1], **Diane Schwegler-Berry**[1], **Anna Shvedova**[1], **Treye Thomas**[3], **Vincent Castranova**[1,4], **Philip Demokritou**[2,*], and **Yong Qian**[1,*]

[1]Pathology and Physiology Research Branch, Health Effects Laboratory Division, National Institute for Occupational Safety and Health, Morgantown, WV 26505, USA

[2]Center for Nanotechnology and Nanotoxicology, Department of Environmental Health, Harvard School of Public Health, Boston, MA 02115, USA

[3]Consumer Product Safety Commission, Office of Hazard Identification and Reduction, Bethesda, MD 20814, USA

[4]Department of Basic Pharmaceutical Sciences, School of Pharmacy, West Virginia University, Morgantown, WV, 26505, USA

Introduction

The use of printers has increased exponentially in the United States over the past few years due to the increase of home offices (Jamieson et. al., 2012). It has been shown in several studies that a laser printer has the ability to increase indoor air particle levels from 860 to 38,000 particles/cm^3 (Barthel et al., 2011, He et al., 2007), with the emitted particles being spherical in shape and having a particle diameter in the range of 50 to 244 nanometers (nm). The majority of the particles are released from various parts of the laser printer, such as the board cooler, rear of the printer, paper tray and toner waste bin (Byeon, 2012, Wang et al., 2012, McGarry et al., 2011, Jiang, 2010, Morawska et al., 2009, Schripp et al., 2008, Wensing et al., 2008, Kagi, 2007, He et al., 2007, Chia-Wei Lee, 2007). The *in vitro* studies performed have used bulk toner particles and concluded that exposures caused delayed pulmonary clearance which led to increased super oxide radicals, cell growth, and cyto and genotoxicity (Furukawa et al., 2002, Mohr U, 2006, Slesinski RS, 2008). Moreover, long-term exposure to the toner material resulted in chronic inflammation, fibrosis and tumor growth in rat lungs (Mohr U, 2006, Morimoto et al., 2005). These studies suggest toxicity of toner powder; however, these results cannot be correlated to exposures at consumer level

*Corresponding Authors. Yong Qian, (304) 285-6286, yaq2@cdc.gov, Philip Demokritou, (617) 432-3481, pdemokri@hsph.harvard.edu.

DECLARATION OF INTEREST STATEMENT

The authors report no competing financial interests.

since the test particles used are not representative of the "real world" exposure to PEPs (Pirela et al., 2014a, Pirela et al., 2014b).

The authors recently developed and utilized a Printer Exposure Generation System (PEGS) to generate, characterize *in situ*, and collect size-fractionated PEPs from 11 commonly used laser printers and ranked them based on their emission profiles. Results show particulate matter (PM) peak emissions from laser printers can reach up to 1.27 million particles/cm^3 with geometric mean diameters ranging from 49 to 208 nm (Pirela et al., 2014a). In a companion paper, the authors confirmed the hypothesis that toner formulations contained ENMs, which are released during printing. A detailed physico-chemical and morphological analysis of both the PEPs and their respective toners, using state of the art technologies, revealed a complex chemistry of organic and inorganic carbon, as well as, several metal/metal oxides (*e.g.*, silica, copper oxide, titanium, nickel, chromium), which correlated with the ENMs present in the toner formulation (Pirela et al., 2014b).

This current manuscript is the first in a series of papers assessing the toxicological properties of the PEPs and possible biological mechanisms of toxicity. Herein, a human alveolar-capillary co-culture model using SAEC and HMVEC was used to determine if different size fractions of PEPs are capable of producing adverse cellular effects on the latter cell line. This co-culture system mimics the alveolar-capillary interaction in the small airways of the lower respiratory tract, reflecting a more physiologically relevant cellular communication. In this study, SAEC were directly treated with non-cytotoxic, low concentrations of 0.5 and 1.0 μg/mL of PEPs ($PM_{0.1}$ and $PM_{2.5}$) for 24 h and then HMVEC were analyzed to determine SAEC-HMVEC communication and the resultant biological responses.

Materials and Methods

Generation and collection of size-fractionated PEPs

The PEPs were generated using the PEGS (Pirela et al., 2014a), a platform recently developed by the authors suitable for the generation and sampling of real world exposures to PEPs. One of the highest emitting printers (referred to as Printer B1 in companion papers), found to emit up to 1.26 million particles/cm^3, was used in this study. Size-selective PM sampling was performed using the Harvard Compact Cascade Impactor (CCI), which collects particles onto impaction substrates in three stages corresponding to $PM_{0.1}$, $PM_{0.1–2.5}$ and $PM_{2.5–10}$ size fractions (Demokritou et al., 2004). After collecting the size-fractionated PM samples, the impaction substrates were removed from the CCI and the particles were extracted using an aqueous suspension methodology (Chang et al., 2013, Pirela et al., 2013a, Bello et al., 2013).

Post sampling characterization of PEPs

Detailed chemical and morphological characterization of PEPs and toner powder for this particular printer, as well as the paper utilized during the study, included testing for total and water-soluble fraction of multiple metals (50 elements), organic and elemental carbon, as well as scanning and transmission electron microscopy (STEM) analysis. Detailed results

from the physico-chemical characterization of PEPs from this high emitting printer are presented in great detail in the companion paper (Pirela et al., 2014b).

Preparation and characterization of particle liquid suspensions for *in vitro* study

Following extraction of PEPs from the CCI impaction substrates, particle dispersions in water were prepared using a protocol developed by the authors (Cohen et al., 2012), which includes the calibration of sonication equipment and standardized reporting of sonication energy. In summary, the critical delivered sonication energy (DSE_{cr}) for each particle used in the study was identified for subsequent sonication and characterization by dynamic light scattering (DLS) to measure hydrodynamic diameter (d_H), polydispersity index (PdI), zeta potential (ζ), and specific conductance (σ). Preparation of all of the particle suspensions was performed just prior to use in the experiments by **c**reating a 1 mg/mL nanoparticle suspension with sterile deionized water (dIH_2O), sonicating at DSE_{cr} and diluting to desired final test concentrations in the respective media. DLS characterization was then repeated to evaluate the properties of the particle in cellular media. Furthermore, colloidal stability of the suspensions, in dIH_2O and in cellular media, was evaluated over various time points following sonication at DSE_{cr}. Subsequently, the effective density of each particle suspension was measured using the volumetric centrifugation method (VCM), recently developed by the authors, as described by Cohen et al. (2012). Effective density is an important determinant of the fate and transport of the agglomerates and *in vitro* dosimetry (see below) (DeLoid et al., 2014, Cohen et al., 2014).

"*In vitro* and *in vivo* dosimetric considerations

It is important to bring *in vivo* and *in vitro* doses on the same scale. Therefore, the dosimetric approach recently developed by the authors was followed (Khatri et al., 2013, Demokritou et al., 2013). In summary, the Multiple-Path Particle Dosimetry 2 (MPPD2) (Anjilvel and Asgharian, 1995) model was used to calculate the dose deposited in the head region, conducting zone, the transitional and respiratory zones of human respiratory system. The airborne nanoparticle distribution values (count median diameter, geometric standard deviation and mass concentration), as well as, the human breathing parameters (tidal volume, breathing frequency, inspiratory fraction, pause fraction, functional residual capacity, head volume and breathing route) listed in Supplemental Table 1 were used in the simulations. It is worth mentioning that the breathing frequency used in the MPPD2 simulation was that of a resting individual (12 breaths/min). Please note that the MPDD2 model provides the deposition mass flux for all the generations of the human respiratory tree.

Thus, the total deposition mass flux of the entire human airways comprised of the conducting zone and the transitional and respiratory zones (excluding the head airway region) was used in the computation of the *in vitro* equivalent volumetric dose, $dose_{in\ vitro,\ eq}$ (μg/mL), which represents dose delivered to cells. It was calculated as follows:

$$\mathrm{dose}_{\mathrm{in\ vitro,eq}} = m_{\mathrm{model}} \times T_{\mathrm{exp}} \times \frac{A_{\mathrm{well}}}{V_{\mathrm{admin}}} \quad (1)$$

Where, $dose_{in\ vitro,\ eq}$ is the equivalent *in vitro* dose (μg/mL), T_{exp} is the total exposure time (min), m_{model} is the sum of each of the MPPD2 model-derived values for mass flux in the conducting, transitional and respiratory zones of the human lung (μg/m^2•min), A_{well} is the surface area of treatment well (m^2) and V_{admin} is the volume of the media in one well (mL).

Subsequently, the hybrid Volumetric Centrifugation Method-*In Vivo* Sedimentation, Diffusion and Dosimetry (VCM-ISDD) methodology recently developed by the authors (DeLoid et al, 2014, Cohen et al, 2014) was used to calculate the fraction of administered *in vitro* particles that deposited to the bottom of the well in a standard 96-well plate as a function of time. For the estimation of the dose delivered to the cell, the agglomerate hydrodynamic diameter, measured by DLS, and the VCM-measured effective density were used as input to the VCM-ISDD model.

Comparative materials

The mild steel welding fumes (WF) were used as a comparative material in this study based upon their complex makeup of metal oxide similar to that of the PEPs. Furthermore, their toxicity in several *in vitro* and *in vivo* studies has been well documented (Antonini et al., 1999, Antonini et al., 2012, Sriram et al., 2012, Zeidler-Erdely et al., 2011). Amorphous silica (SiO_2), which was previously characterized, was also used as a comparative nanomaterial (Cohen et al., 2013, Gass et al., 2013).

Cell Culture

SAEC were a gift from Dr. Tom K. Hei (Columbia University, New York, NY) and were cultured as previously described (Piao et al., 2005). Briefly, the SAEC were cultured in serum free Small Airway Epithelial Cell growth medium (SABM) with the addition of multiple supplemental growth factors (Bovine Pituitary Extract, Hydrocortisone, Human Epidermal Growth Factor, Epinephrine, Transferrin, Insulin, Retinoic, Triiodothyronine, Gentimicin Amphoteracin-B, and Bovine serum Albumin-fatty acid free (BSA-FAF) provided by the manufacturer (Lonza, Inc. Allendale, NJ). The HMVEC were gifted by Dr. Rong Shao (BioMedical Research Institute, Baystate Medical Center, University of Massachusetts, Amherst, MA) and have been described previously (Shao and Guo, 2004). HMVEC were cultured in endothelial basal medium-2 (EBM-2) (Lonza, Inc. Allendale, NJ) with the addition of 10% fetal bovine serum (FBS) (Atlanta Biological, Lawrencville, GA), 100 U/mL penicillin and 10 μg/mL streptomycin (Lonza, Inc. Allendale, NJ), 0.01 μg/mL epidermal growth factors (EGF) (Sigma, St. Louis, MO), and 1 μg/mL hydrocortisone (Sigma, St. Louis, MO). Cells were maintained at 37°C with 5% carbon dioxide.

Details of the *in vitro* alveolar-capillary co-culture model, summarized in Supplemental Figure 1, were previously published (Snyder-Talkington BN, 2013). Briefly, 6-well polyester 0.4-μm pore size transwells (Corning Inc., NY, USA) were hydrated with SABM for at least 1 h in a secondary 6-well plate. HMVEC (2.25×10^5cells per well) were plated with or without a coverslip. HMVEC were fully attached before the addition of the transwell insert. Then SAEC were plated at 1.5×10^5 cells per well and allowed to fully attach for 24 h, followed by media changes to remove any dead cells in both chambers. At 48 h, each of the

chambers was serum starved for an additional 24 h then treated with PEPs for 24 h and then assayed.

Cytotoxicity of SAEC

SAEC were plated at 1.5×10^4 cells per well in a 96 well plate (BD Biosciences, NJ, USA) The Cell Titer 96 ® Aqueous One Solution Cell Proliferation Assay Kit (Promega, WI, USA) was used to determine the changes in cell proliferation according to the manufacturer's protocol. The following concentrations were used to determine cytotoxicity in the MTS Assay: 0.0 μg/mL, 0.5 μg/mL, 1.0 μg/mL, and 2.5 μg/mL.

Transmission Electron Microscopy

Following treatment with PEPs $PM_{0.1}$ for 24 h, SAEC were fixed in Karnovsky's fixative (2.5% glutaldehyde, 2.5% paraformaldehyde in 0.1M Sodium Cacodylic buffer). HMVEC on the bottom chamber of the transwells were trypsinized and centrifuged at 1,000 × g for 5 min at room temperature and then fixed with Karnovsky's fixative. SAEC and HMVEC samples were post-fixed in osmium tetroxide, mordanted in 1% tannic acid and stained in bloc in 0.5% uranyl acetate. The samples were embedded in epon, sectioned and stained with Reynold's lead citrate and uranyl acetate. The sections were imaged on a JEOL 1220 transmission electron microscope.

Cytokine and Chemokine Analysis

The SAEC and HMVEC cellular lysates were collected following the protocol from the Bio-Plex ™Cell Lysis Kit (Bio Rad, CA, USA). Both the condition media and cellular lysates were analyzed for 27 cytokines and chemokines using the Bio-Plex Pro Human Cytokine 27-Plex Assay (Bio-Rad, CA, USA) after the co-cultured SAEC were treated with dI H_2O, PEPs $PM_{0.1}$ 1.0 μg/mL, SiO_2 1.0 μg/mL, or WF 1.0 μg/mL for 24 h. The samples were run on the Bio-Plex®200 System and analyzed using Bio-Plex Manager™ 6.0 software. Cytokines and Chemokines that were elevated within the PEPs $PM_{0.1}$ are shown in Figure 6; however, the following cytokines and chemokines were included in the Bio-Plex: (IL-1β, IL-rα, IL-2, IL-4, IL-5, IL-6, IL-7, IL-8, IL-9, IL-10, IL-12p70, IL-13, IL-15, IL-17A, Ecotaxin, Basic FGF, G-CSF, GM-CSF, IFN-γ, IP-10, MCP-1, MIP-1α, MIP-1β, PDGF-BB, RANTES, TNF-α, and VEGF.

Confocal Microscopy

To measure the amount of ROS, 5 μM final concentration of dihydroethidum (DHE) (Invitrogen, NY, USA) was added to the HMVEC media during the last 30 min of the PEPs treatment. To confirm the production of ROS, the HMVEC were pretreated with 2,000 U/mL catalase (Sigma, MO, USA) for 1 h to scavenge the ROS. The cells on the coverslips were fixed with 3.6% paraformaldehyde and washed three times with 1 × PBS. The cells were mounted and imaged with a confocal microscope (Zeiss, Germany).

Change in actin filaments and gap formation were measured in the HMVEC monolayer. The HMVEC on the coverslips were fixed with 3.6% paraformaldehyde and permeabilized with 0.1% triton x-100/PBS. Samples were blocked in 3% BSA (Fisher Scientific, PA, USA) and washed three times with 1 × PBS. HMVEC were stained with phalloidin (AlexaFluor 546,

Invitrogen, NY, USA) for actin filaments and rabbit anti-VE cadherin (Alexis Biochemicals, San Diego, CA). Samples were incubated with secondary anti-rabbit Alexa Fluor 647 (Invitrogen, NY, USA) mounted with ProLong Gold anti-fad (Invitrogen, NY, USA) and imaged using a Zeiss LSM510 microscope. Scale bars were generated and inserted using LSM software.

Angiogenesis Assay

SAEC and HMVEC were grown in the co-culture system to 90–100% confluence and were exposed to PEPs for 24 h. After the treatment, HMVEC were trypsinized and 6.0×10^4 HMVEC were plated on 2 mg/mL matrigel (BD Biosciences, CA, USA) in a 24-well plate. The cells were imaged every 30 min for 4 h to measure tube formation. The images were taken on the Spot/retiga at both 4× and 10×. Tube formation was quantified using the 10× images.

Statistics

Experiments were performed in biological triplicates and expressed with the standard error. Images are a representation of n = 3. Student t-test was used to determine significance set at $p < 0.05$.

Results

Physicochemical properties of collected PEPs

In the two companion papers, we show in detail the characterization of toner powder and PEPs from 11 commonly used laser printers (Pirela et al., 2014a, Pirela et al., 2014b). In summary, the “high emitting” laser printer used in this study (referred to as Printer B1 in our previous publications) released up to 1.26 million particles/cm^3 during a 1 h, continuous print job. The emitted PM had a unimodal size distribution and aerodynamic diameters that ranged from 39 to 122 nm. STEM/EDX analysis of both the toner powder and PEPs showed presence of ENMs in the toner that became airborne during printing. Further chemical analysis revealed a similar complex chemical fingerprint between the toner and PEPs, with PEPs containing 42% carbon, 1.5% metal (*e.g.*, aluminum, titanium, cerium, zinc and copper) and 56% other (*e.g.*, phosphorus, sulfur, chlorine) (Pirela et al., 2014b).

Sampled PEPs dispersion and characterization in liquid suspensions

Table 1 summarizes the particle agglomerate colloidal behavior in both dIH_2O and small airway basal medium (SABM), as described by hydrodynamic diameter (d_H), zeta potential (ζ), polydispersity index (PdI) and specific conductance (σ). Observed values of ζ were strongly negative for the $PM_{0.1}$ PEPs size fraction in dIH_2O (−20.6 mV) and became positive when dispersed in SABM (9.97 mV). The opposite was observed for the larger PEPs counterpart ($PM_{2.5}$), whose ζ was −16 mV in dIH_2O and remained negative when suspended in SABM (−17.7 mV). The WF, used here as a comparator material of known toxicity, were determined to have a d_H of 2197 nm in dIH_2O, which decreased to 1878 nm when dispersed in SABM. Lastly, the d_H of silica increased dramatically from 142.5 nm (in dIH_2O) to 663.8 nm (in SABM). The colloidal stability of the particle suspensions was subsequently evaluated 24 h post-sonication to DSE_{cr}. The d_H of PEPs ($PM_{0.1}$) suspended in

SABM remained stable with an average diameter ranging from 200 to 250 nm (data not shown). Contrasting stability was observed for the bigger size fraction of PEPs ($PM_{2.5}$), whose d_H increased substantially at 10 h post-sonication going from approximately 200 nm to 600 nm (data not shown). SiO_2 and WF also remained as a stable dispersion for up to 24 h. Thus, in order to maintain the most stable particle suspension, the dispersions were always prepared and sonicated at DSE_{cr} immediately prior to cell treatment.

The VCM measured effective density of the ENMs suspensions and results show that the smallest size fraction of PEPs ($PM_{0.1}$) had an effective density of 2.39 g/cm^3, lower than that of the larger size fraction of PEPs ($PM_{2.5}$) of 3.10 g/cm^3. The effective densities of the comparator materials used in the study were 1.2 g/cm^3 for silica and 1.37 g/cm^3 for WF.

Dosimetric considerations for *in vitro* testing

In order to ensure that the *in vitro* doses used in this study are equivalent to current consumer exposures to PEPs, the total human lung deposited dose for a corresponding consumer inhalation exposure duration was determined using the MPPD2 model as described in the methods section. The *in vitro* equivalent volumetric dose, $dose_{in\ vitro,\ eq}$, (μg/mL), estimated using the total lung deposition mass flux (1.732 μg/m^2•min) was found to be 0.485, 3.88 and 11.65 μg/mL for exposure durations of 1, 8 and 24 hours of corresponding inhalation to PEPs, respectively.

Furthermore, the administered dose which is deposited on the cells on the bottom of the well for PEPs $PM_{0.1}$, PEPs $PM_{2.5}$ and comparative materials was calculated as briefly described in the methods and presented in Supplemental Figure 2. The delivered to cell dose at a given exposure time-point is not always the same as the dose administered (Cohen et. al., 2013) as it depends on the effective density and size of the formed agglomerates and partico-kinetics in general in the *in vitro* system, which can have serious implications on toxicological ranking of nanomaterials *in vitro* (Cohen et. al., 2014). The estimated fraction of administered particle mass that reaches the bottom of the well in the chosen experimental exposure duration for each particle suspension is summarized in Supplemental Table 2. Results show that it will take less than two hours for all of the administered WF mass to deposit. However, the opposite is observed for SiO_2, as only approximately 40% of the administered dose will actually reach the bottom of the well. Interestingly, for a 24 h *in vitro* exposure duration, both PEPs size fractions, 100% of the administered dose will be deposited to the cells at the bottom of the well (Supplemental Figure 3). It is worth noting that the fate and transport of formed agglomerates in the *in vitro system* is defined by two fundamental parameters, namely the diameter of the formed agglomerate as well as their effective density (Deloid et al, 2014; Cohen et al, 2014). In this particular PM suspensions, the combinations of diameter and effective density of the formed agglomerates in the media resulted to faster deposition of the $PM_{0.1}$ size fraction compared to the larger PEPs ($PM_{2.5}$) due to higher agglomerate diameter for PEPs $PM_{0.1}$. The corresponding equivalent consumer inhalation exposure duration (hours), and the associated delivered to cell doses used in the study are presented in Supplemental Table 2.

PEPs induce cytotoxicity in SAEC

Supplemental Figure 4 illustrates the results from the MTS assay. Results indicate that the $PM_{0.1}$ size fraction of PEPs and WF were toxic to SAEC at the administered dose of 2.5 μg/mL. Although, PEPs ($PM_{2.5}$) and SiO_2 were not toxic at 2.5 μg/mL, they caused an increase in metabolic activity. At the low concentration of 1.0 μg/mL, PEPs ($PM_{0.1}$) or PEPs ($PM_{2.5}$) showed no significant changes in metabolic activity or cytotoxicity. There were also no significant changes seen when SAEC were treated with 0.5 μg/mL of any of the nanoparticles. Therefore, the non-cytotoxic levels of 0.5 μg/mL and 1.0 μg/mL were used for the remaining studies utilizing the co-culture model.

PEPs are engulfed by SAEC but did not reach HMVEC

In this study, the SAEC-HMVEC *in vitro* alveolar-capillary co-culture model was applied to identify cellular effects induced by different size fractions of PEPs. SAEC on the transwell membrane were exposed to PEPs directly, and the underlying HMVEC in the basolateral section were subjected to multiple assays. Therefore, it was of importance to determine the location of the PEPs within the SAEC-HMVEC co-culture model by TEM. As seen in Figure 1, SAEC engulfed the PEPs after a 24 h treatment. It appears that the PEPs were not able to translocate to the basolateral chamber, suggesting that the HMVEC did not have direct interaction with PEPs. Therefore, it can be hypothesized that the endothelial cellular effects observed in this co-culture model are mainly due to the cellular communication between the epithelial and endothelial cells caused by PEPs and not direct HMVEC interaction with PEPs.

PEPs increase ROS in HMVEC

Nanomaterials have been shown to cause an increase in the production of ROS *in vivo* and *in vitro*, which has been linked to nanoparticle-induced toxic effects (Sotiriou et al., 2012, Demokritou et al., 2013, Nel A, 2006). HMVEC were examined to determine their ability to produce ROS upon co-culture with SAEC exposed to PEPs. As can be seen in Figure 2, there was an increase in ROS production in HMVEC when SAEC were treated with either PEPs $PM_{0.1}$ 1.0 μg/mL (C), PEPs $PM_{2.5}$ 1.0 μg/mL (D), SiO_2 1.0 μg/mL (E) or WF 1.0 μg/mL (F). Comparison of the intensities among these treatments, indicates that exposure to PEPs $PM_{0.1}$ 1.0 μg/mL induced the highest amount of ROS even when compared to cells treated with WF. However, there does not appear to be an increase in ROS with PEPs $PM_{0.1}$ at 0.5 μg/mL compared to the control. To confirm production of ROS, HMVEC were pretreated with catalase, a ROS scavenger, as illustrated in Figure 2 (G-L) resulted in blocking ROS production.

PEPs increase morphological changes in HMVEC

To determine if the treatment of SAEC with PEPs caused morphological changes to the endothelial monolayer, HMVEC were fixed and stained with FITC-phalloidin for actin filaments, as described in the methods. As seen in Figure 3, there is an increase in the remodeling of actin filaments in HMVEC after treatment of SAEC with PEPs $PM_{0.1}$ at 1.0 μg/mL and PEPs $PM_{2.5}$ at 1.0 μg/mL. Results show that PEPs $PM_{0.1}$ and $PM_{2.5}$ increased cell motile structures in HMVEC, such as stress fibers, filopodia and lamellipodia.

VE-cadherin expression is specific to endothelial cells and is necessary within the adheren junctions to maintain cellular contact within the endothelial monolayer (Mehta and Malik, 2006). To determine the integrity of the endothelium upon co-culturing with PEPs-treated SAEC, HMVEC were fixed and stained with VE-cadherin antibody. PEPs $PM_{0.1}$ 0.5 μg/mL did not change gap formation (Figure 4B). There were increased gap junctions in the PEPs $PM_{0.1}$ 1.0 μg/mL endothelium in comparison to the WF 1.0 μg/mL. PEPs $PM_{2.5}$ 1.0 μg/mL (Figure 4D) showed an increase in gap formation; however, it induced less gap formation than PEPs $PM_{0.1}$ 1.0 μg/mL. The SiO_2 did not increase gap formation compared to control while the WF did (Figure 4E and 4F). These results demonstrated that SAEC exposure to PEPs induced morphological changes of HMVEC in the co-culture model.

PEPs increase angiogenesis HMVEC

To determine if SAEC exposure to PEPs would increase angiogenesis in HMVEC, an *in vitro* matrigel endothelial tube formation assay was performed. As seen in Figure 5 and Supplemental Figure 5, there was an increase in tube formation with PEPs $PM_{0.1}$ 0.5 μg/mL and 1.0 μg/mL compared to control and PEPs $PM_{2.5}$ 1.0 μg/mL. The 1.0 μg/mL SiO_2 nanoparticles did not increase tube formation in the HMVEC; however, it can be seen that the 1.0 μg/mL WF did increase the number of tubes. These data demonstrate that SAEC exposure to PEPs $PM_{0.1}$ at both 0.5 μg/mL and 1.0 μg/mL has the ability to increase angiogenesis in HMVEC within the co-culture model.

PEPs induce secretion of inflammatory mediators

To determine whether SAEC exposure to PEPs induce cellular communication within the co-culture system, a panel of 27 cytokines and chemokines were measured in both the conditioned media and cellular lysates of each cell type. After a 24 h treatment with PEPs $PM_{0.1}$, SAEC-conditioned media had significantly elevated levels of IL-1β, IL-1rα and IL-6 compared to the control (Figure 6A). It can be seen that WF also increased levels of IL-1β and IL-6 but there was no significant difference between control and SiO_2. As for the SAEC cellular lysates, the following cytokines were all significantly elevated post-exposure to PEPs $PM_{0.1}$ when compared to control (Figure 6B): IL-6, IL-8, basic fibroblast growth factors (FGF basic), interferon gamma induced protein 10 (IP-10), monocyte chemotactic protein-1 (MCP-1) and RANTES. The SiO_2-treated SAEC cellular lysates induced an increase in MCP-1 and RANTES when compared to control. As seen in Figure 6C, the HMVEC-conditioned media showed significant increase in IL-6, MCP-1, and a decrease in MIP-1b in the PEPs $PM_{0.1}$ group when compared to control. The only significant change that occurred in the conditioned media of the comparative nanomaterial was a decrease in IL-6 with the SiO_2 group. To determine if the HMVEC produced any cytokines or chemokines post-indirect exposure to PEPs $PM_{0.1}$, cellular lysates of the HMVEC were also analyzed using the same 27-member panel. As seen in Figure 6D, the only inflammatory mediator that was elevated within the HMVEC cellular lysate was IL-8, which remained unchanged within SiO_2 and WF. These data demonstrate that there is a specific cytokine and chemokine profile that is induced in HMVEC upon SAEC treatment with PEPs $PM_{0.1}$ in the co-culture model. Therefore, it can be concluded that IL-1β, IL-1rα, and IL-6 were all elevated in the SAEC conditioned media while IL-6, IL-8, FGF basic, IP-10, MCP-1 and RANTES were significantly elevated in the SAEC cellular lysates. Within the HMVEC

conditioned media IL-6, MCP-1 and MIP-1b were all elevated while only IL-8 was elevated within the HMVEC cellular lysates.

Discussion

The current study provides evidence that PEPs are bioactive and to our knowledge is the first study that has focused on the toxicity of low concentrations (0.5 μg/mL and 1.0 μg/mL) of real world PEPs instead of the starting bulk toner powder. With the use of the *in vitro* alveolar-capillary unit we were able to demonstrate that PEPs induce cellular communication between the exposed SAEC and the underlying HMVEC. This is an important model to study because it mimics the cellular crosstalk in the alveolar capillary unit upon a nanoparticle inhalation exposure, which is a limitation of mono-culture systems. Upon indirect treatment of PEPs, the endothelium was shown to be disrupted through actin remodeling and gap junctions, which has been linked previously to inflammation.(Mehta and Malik, 2006). It was also determined that PEPs have the ability to induce ROS in the underlying HMVEC most likely due to the metal content within their complex makeup. Upon further evaluation, PEPs induced an inflammatory response through the activation of cytokines and chemokines, which lead to the crosstalk between SAEC and HMVEC.

Printers have become a standard commodity within offices, homes, schools, and many other indoor environment over the past decade. In our two companion papers on the physico-chemical and morphological properties of PEPs and toner formulations, we provide evidence that current toners constitute a NEP and contain ENMs that are subsequently released into the air during consumer use (Pirela et al., 2014b). In particular, the PEPs and toner powder from the printer used in this study shared a complex chemical composition that included a large percentage of organic and elemental carbon, as well as, inorganic elements such as magnesium, aluminum, titanium, iron, cobalt, nickel, copper and zinc, among others. Most of these ENMs released in the air are known to produce negative biological responses in different testing platforms including lung injury and inflammation, as well as, DNA damage (Watson et al., 2014, Demokritou et al., 2013) and it can be hypothesized based upon this information that the PEPs bioactivity that led to the disruption of the endothelium after epithelial exposure was due to their metal content. To this regard, this study is of paramount importance because it provides evidence that humans are exposed to nanoscale materials released from NEPs during consumer use and those real world exposures may have serious toxicological implications. More importantly, this study illustrates the importance of utilizing the real world exposures across life cycle rather than using the raw material properties for nano-risk assessment studies.

Last but not least, in this study, the *in vitro* alveolar-capillary model of SAEC-HMVEC co-culture was applied to understand the mechanism of PEPs-induced toxicity. It was demonstrated for the first time that PEPs exposure at very low levels altered cellular communication between SAEC and HMVEC. The cellular communication between epithelial and endothelial cells within the lung plays a major role in the pathogenesis of pulmonary inflammation, fibrosis, and cancer (Homer et al., 2011, Hoo and Whyte, 2012, Kuebler, 2005, Strieter and Mehrad, 2009, Wallace et al., 2007). This model represents the alveolar-capillary unit, which is the major site of gas exchange within the lung. Damage of

this critical pulmonary site due to particle exposure can lead to pulmonary inflammation, fibrosis, decreased gas exchange, and other diseases (Wallace et al., 2007, Strieter and Mehrad, 2009). The use of the co-culture model which allows for the study of epithelial and endothelial cellular communication within the alveolar-capillary unit, offers an advantage over mono-culture cell models commonly used in nanotoxicology studies. It is worth nothing that a comparative study recently performed by our group showed that the *in vitro* alveolar-capillary co-culture model correlates with *in vivo* results more closely than a mono-culture model upon treatment with multi-walled carbon nanotubes (MWCNT) (Snyder-Talkington BN, 2012).

It is worth nothing that SAEC exposure levels were low and equivalent to PEPs inhalation of 1 to 2 h. To our knowledge, this is the first publication that links such a low, non-cytotoxic exposure dose (0.5 μg/mL and 1.0 μg/mL) to toxicological effects. Additionally, based upon TEM analysis, it was determined that the underlying HMVEC did not have direct contact with PEPs, which is consistent with findings from a MWCNT exposure in co-culture model (Snyder-Talkington BN, 2013). In summary, it was clearly demonstrated in this study that the observed biological response seen in the underlying HMVEC in the SAEC-HMVEC co-culture model is independent of cell death signaling.

One possible mechanism for the cellular cross-talk is through the expression of cytokines and chemokines. Our results showed that IL-6 was significantly elevated in both the conditioned media of the SAEC and HMVEC, but its expression was only found significantly increased in the cellular lysates of SAEC and not of HMVEC. IL-6 is known to be a pro-inflammatory cytokine that plays a major role in the acute and chronic immune responses by activating pathways that control proliferation, differentiation migration and apoptosis (Maruo et al., 1992, Scheller et al., 2014). It was also noted that MCP-1, also known as CCL2, was elevated within both the cellular lysates of epithelial exposed PEPs and the conditioned media of the underlying endothelial cells. MCP-1 regulates the migration and infiltration of macrophages and monocytes during an immune response and has been linked to multiple disease states, such as pulmonary disease (Deshmane et al., 2009). Both IL-6 and MCP-1 have been directly linked to the activation of endothelial cells resulting in increased angiogenesis and membrane permeability (Garcia-Roman and Zentella-Dehesa, 2013, Middleton et al., 2014, Cromer et al., 2014). These data suggests that the cellular communication is being mediated by both IL-6 and MCP-1. This correlates with findings from a series of *in vivo* an *in vitro* studies evaluating the toxicity of copier-emitted particles (Pirela et al., 2013b, Khatri M, 2013b, Khatri M, 2013a) and studies that linked the expression of MCP-1 to fibrosis in an *in vivo* MWCNT study (Snyder-Talkington et al., 2013). It can be concluded here that the alterations seen in the endothelium upon SAEC PEPs exposure is linked to the inflammatory signaling of IL-6 and MCP-1. ICAM-1 and VCAM-1 are adhesion molecules in their soluble form that play a key role within the interaction of leukocytes and endothelial cells (Muller, 2011). It has been previously published that both soluble ICAM-1 and VCAM-1 play a major role in elevated inflammatory response and endothelial dysfunction (Lawson and Wolf, 2009). It is worth nothing that both ICAM-1 and VCAM-1 have been shown to be elevated upon particle

exposure (Snyder-Talkington BN, 2013, Pirela et al., 2013a). We will also focus on ICAM-1 and VCAM-1 in the next phase of our search, which focuses on *in vivo* mouse exposures.

In this study, it was also demonstrated that PEPs exposed SAEC induced an up-regulation of ROS production in HMVEC, which is consistent with the results of IL-6 expression since it induces ROS to activate various molecular pathways (Szmitko et al., 2003). It has been well demonstrated that nanoparticle exposure induces the production of ROS (Nel A, 2006, Roy et al., 2014, Kovacic P, 2013, Apopa PL, 2009). The increase in the production of ROS within a cell can lead to damage of DNA, proteins or lipids (Watson et al., 2014). ROS are the term used for the intermediate forms of aerobic metabolism, which includes superoxide ($O_2^{\cdot}$), hydrogen peroxide (H_2O_2), hydroxyl radical ($^{\cdot}OH$) and peroxynitrite ($ON_2^{\cdot}$) (Rahal et al., 2014). Studies have shown that increased ROS production is related to interruption of the endothelial monolayer and pulmonary hypertension within the lungs (Roberts et al., 2010, Tabima et al., 2012). Indicating that epithelial exposure to PEPs has the ability to increase the ROS production in the underlying endothelial cells, which may lead to a disruption in the endothelial monolayer.

Another interesting finding of this study is the fact that epithelial cell exposure to PEPs induced endothelial cell permeability and angiogenesis. The vascular endothelial monolayer forms a semi-selective permeability barrier between blood and interstitial space to control the movement of proteins, macromolecules, and water across the vessel wall. The preservation of the endothelial monolayer is important to maintain gas exchange function of alveolar-capillary units. Aberrations of the permeability barrier integrity may lead to damage of alveolar-capillary units, which can play a major role in the pathogenesis of fibrosis, angiogenesis, cardiovascular diseases, inflammation, and acute lung injury syndromes (Mehta and Malik, 2006). Angiogenesis is the process of new blood vessel formation, which involves vascular permeability, growth factors recruitment, migration, proliferation and tube formation. The process of increasing angiogenesis is associated with cancer, cardiovascular diseases and chronic inflammation (Bryan and D'Amore, 2007, Adams and Alitalo, 2007, Griffioen and Molema, 2000). Results from this study strongly indicate that cellular signaling from epithelial exposed PEPs induces endothelial angiogenesis through IL-6 and MCP-1 pathways (Garcia-Roman and Zentella-Dehesa, 2013, Middleton et al., 2014, Cromer et al., 2014). Moreover, the production of IL-6 has been shown to produce cytosolic IL-8 within endothelial cells to increase angiogenesis (Volk et al., 2000). Indeed, our results show that PEPs-exposed SAEC up-regulates the production of IL-8 in the HMVEC cellular lysate. Therefore it can be concluded that the cytokine and chemokine signaling cascade from PEPs-exposed SAEC is a key step in the cellular alterations seen in the underlying HMVEC.

Conclusion

This study, along with the companion studies on the physico-chemical characteristics of nanoparticles released from toner during consumer use (printing), is the first to demonstrate that the ENMs that are incorporated into the toner are emitted during the use of a laser printer and have bioactive properties. This study provides important findings on the mechanistic pathways of observed bioactivity and demonstrates that exposure of SAEC to

different size fractions of PEPs at doses comparable to current inhalation exposures at consumer level, induces adverse effects to the underlying HMVEC through cellular communication. The results indicate that the adverse endothelial effects could be due to cellular signals of IL-6 and MCP-1 from the epithelial cells. Demonstration of adverse effects caused by exposure to PEPs in an *in vitro* co-culture model justifies further *in vivo* and *in vitro* toxicological studies of PEPs.

Supplementary Material

Refer to Web version on PubMed Central for supplementary material.

Acknowledgments

The authors acknowledge funding for this study from NIEHS (Grant # ES-000002) and NIOSH and CPSC (Grant # 212-2012-M-51174).

The findings and conclusion in the report are of the authors and do not necessarily represent the views of the National Institute for Occupational Safety and Health.

References

Adams RH, Alitalo K. Molecular regulation of angiogenesis and lymphangiogenesis. Nat Rev Mol Cell Biol. 2007; 8:464–478. [PubMed: 17522591]

Anjilvel S, Asgharian B. A MULTIPLE-PATH MODEL OF PARTICLE DEPOSITION IN THE RAT LUNG. Fundamental and Applied Toxicology. 1995; 28:41–50. [PubMed: 8566482]

Antonini J, Lawryk N, Murthy G, Brain J. Effect of welding fume solubility on lung macrophage viability and function in vitro. J Toxicol Environ Health A. 1999; 58:343–363. [PubMed: 10580758]

Antonini J, Zeidler-erdely P, Young S, Roberts J, Erdely A. Systemic immune cell response in rats after pulmonary exposure to manganese-containing particles collected from welding aerosols. J Immunotoxicol. 2012; 9:184–192. [PubMed: 22369286]

Apopa pl QY, Shao R, Guo NL, Schwegler-berry D, Pacurari M, Porter D, Shi X, Vallyathan V, Castranova V, Flynn DC. Iron oxide nanoparticles induce human microvascular endothelial cell permability through reactive oxygen species production and microtubule remodeling. Particle and Fibre Toxicology. 2009

Barthel M, Pedan V, Hahn O, Rothhardt M, Bresch H, Jann O, Seeger S. XRF-analysis of fine and ultrafine particles emitted from laser printing devices. Environ Sci Technol. 2011; 45:7819–7825. [PubMed: 21809840]

Bello D, Martin J, Santeufemio C, Sun QW, Bunker KL, Shafer M, Demokritou P. Physicochemical and morphological characterisation of nanoparticles from photocopiers: implications for environmental health. Nanotoxicology. 2013; 7:989–1003. [PubMed: 22551088]

Bryan BA, D'amore PA. What tangled webs they weave: Rho-GTPase control of angiogenesis. Cell Mol Life Sci. 2007; 64:2053–2065. [PubMed: 17530172]

Byeon JH, Kim J-W. Particle emission from laser printers with different printing speeds. Atmospheric Environment. 2012; 54:272–276.

Chang CL, Demokritou P, Shafer M, Christiani D. Physicochemical and toxicological characteristics of welding fume derived particles generated from real time welding processes. Environmental Science-Processes & Impacts. 2013; 15:214–224. [PubMed: 24592438]

Chia-wei Lee D-JH. Measurements of fine and ultrafine particles formtion in photocopy centers in Taiwan. Atmospheric Environment. 2007; 41:6598–6609.

Cohen J, Deloid G, Pyrgiotakis G, Demokritou P. Interactions of engineered nanomaterials in physiological media and implications for in vitro dosimetry. Nanotoxicology. 2012

Cohen J, Deloid G, Pyrgiotakis G, Demokritou P. Interactions of engineered nanomaterials in physiological media and implications for in vitro dosimetry. Nanotoxicology. 2013; 7:417–431. [PubMed: 22393878]

Cohen JM, Teeguarden JG, Demokritou P. An integrated approach for the in vitro dosimetry of engineered nanomaterials. Part Fibre Toxicol. 2014; 11:20. [PubMed: 24885440]

Cromer WE, Zawieja SD, Tharakan B, Childs EW, Newell MK, Zawieja DC. The effects of inflammatory cytokines on lymphatic endothelial barrier function. Angiogenesis. 2014; 17:395–406. [PubMed: 24141404]

Deloid G, Cohen JM, Darrah T, Derk R, Rojanasakul L, Pyrgiotakis G, Wohlleben W, Demokritou P. Estimating the effective density of engineered nanomaterials for in vitro dosimetry. Nat Commun. 2014; 5(3514)

Demokritou P, Gass S, Pyrgiotakis G, Cohen JM, Goldsmith W, Mckinney W, Frazer D, Ma J, Schwegler-berry D, Brain J, Castranova V. An in vivo and in vitro toxicological characterisation of realistic nanoscale CeO(2) inhalation exposures. Nanotoxicology. 2013; 7:1338–1350. [PubMed: 23061914]

Demokritou P, Lee SJ, Ferguson ST, Koutrakis P. A compact multistage (cascade) impactor for the characterization of atmospheric' aerosols. Journal of Aerosol Science. 2004; 35:281–299.

Deshmane SL, Kremlev S, Amini S, Sawaya BE. Monocyte chemoattractant protein-1 (MCP-1): an overview. J Interferon Cytokine Res. 2009; 29:313–326. [PubMed: 19441883]

Furukawa Y, Aizawa Y, Okada M, Watanabe M, Niitsuya M, Kotani M. Negative effect of photocopier toner on alveolar macrophages determined by in vitro magnetometric evaluation. Ind Health. 2002; 40:214–221. [PubMed: 12064564]

Garcia-roman J, Zentella-dehesa A. Vascular permeability changes involved in tumor metastasis. Cancer Lett. 2013; 335:259–269. [PubMed: 23499893]

Gass S, Cohen JM, Pyrgiotakis G, Sotiriou GA, Pratsinis SE, Demokritou P. A Safer Formulation Concept for Flame-Generated Engineered Nanomaterials. ACS Sustain Chem Eng. 2013; 1:843–857. [PubMed: 23961338]

Griffioen AW, Molema G. Angiogenesis: potentials for pharmacologic intervention in the treatment of cancer, cardiovascular diseases, and chronic inflammation. Pharmacol Rev. 2000; 52:237–268. [PubMed: 10835101]

He C, Morawska L, Taplin L. Particle emission characteristics of office printers. Environ Sci Technol. 2007; 41:6039–6045. [PubMed: 17937279]

Homer RJ, Elias JA, Lee CG, Herzog E. Modern concepts on the role of inflammation in pulmonary fibrosis. Arch Pathol Lab Med. 2011; 135:780–788. [PubMed: 21631273]

Hoo ZH, Whyte MK. Idiopathic pulmonary fibrosis. Thorax. 2012; 67:742–746. [PubMed: 21697287]

Jamieson L. Ink and Toner Cartridge Use among SMBs in the United States. Photizo Group. 2012

Jiang HALL. Measurement of the surface charge of ultrafine particles from laser printers and analysis of their electrostatic force. Atmospheric Environment. 2010; 44:3347–3351.

Kagi N, Fuji S, Horiba Y, Namiki N, Ohtani Y, Emi H, Tamura H, Kim YS. Indoor air quality for chemical and ultrafine particle contaminants from printers. Building and Environment. 2007; 42:1949–1954.

Khatri MBD, Pal A, Cohen J, Woskie S, Gassert T, Lan J, Gu A, Demokritou P, Gaines P. Evaluation of cytotoxic, genotoxic and inflammatory responses of nanoparticles from photocopiers in three human cell lines. Particle and Fibre Toxicology. 2013a; 10

Khatri MBD, Pal A, Woskie S, Gassert T, Demokritou P, Gaines P. Toxicological effects of PM0.1-2.5 particles collected from a photocopy center in three human cell lines. Inhalation Toxicology. 2013b; 25:621–632. [PubMed: 24044678]

Khatri M, Bello D, Pal AK, Cohen JM, Woskie S, Gassert T, Lan JQ, Gu AZ, Demokritou P, Gaines P. Evaluation of cytotoxic, genotoxic and inflammatory responses of nanoparticles from photocopiers in three human cell lines. Particle and Fibre Toxicology. 2013; 10

Kovacic PSR. Nanoparticles: toxicity, radicals, electron transfer, and antioxidants. Methods Mol Biol. 2013

Kuebler WM. Inflammatory pathways and microvascular responses in the lung. Pharmacol Rep. 2005; 57(Suppl):196–205. [PubMed: 16415500]

Lawson C, Wolf S. ICAM-1 signaling in endothelial cells. Pharmacol Rep. 2009; 61:22–32. [PubMed: 19307690]

Maruo N, Morita I, Shirao M, Murota S. IL-6 increases endothelial permeability in vitro. Endocrinology. 1992; 131:710–714. [PubMed: 1639018]

Mcgarry P, Morawska L, He C, Jayaratne R, Falk M, Tran Q, Wang H. Exposure to particles from laser printers operating within office workplaces. Environ Sci Technol. 2011; 45:6444–6452. [PubMed: 21662984]

Mehta D, Malik AB. Signaling mechanisms regulating endothelial permeability. Physiol Rev. 2006; 86:279–367. [PubMed: 16371600]

Middleton K, Jones J, Lwin Z, Coward JI. Interleukin-6: an angiogenic target in solid tumours. Crit Rev Oncol Hematol. 2014; 89:129–139. [PubMed: 24029605]

Mohr UEH, Roller M, Pott F. Pulmonary tumor types induced in wistar rats of the co-called "19-dust study". Exp Toxicol Pathol. 2006; 58:13–20. [PubMed: 16806863]

Morawska L, He C, Johnson G, Jayaratne R, Salthammer T, Wang H, Uhde E, Bostrom T, Modini R, Ayoko G, Mcgarry P, Wensing M. An investigation into the characteristics and formation mechanisms of particles originating from the operation of laser printers. Environ Sci Technol. 2009; 43:1015–1022. [PubMed: 19320151]

Morimoto Y, Kim H, Oyabu T, Hirohashi M, Nagatomo H, Ogami A, Yamato H, Obata Y, Kasai H, Higashi T, Tanaka I. Negative effect of long-term inhalation of toner on formation of 8-hydroxydeoxyguanosine in DNA in the lungs of rats in vivo. Inhal Toxicol. 2005; 17:749–753. [PubMed: 16195210]

Muller WA. Mechanisms of leukocyte transendothelial migration. Annu Rev Pathol. 2011; 6:323–344. [PubMed: 21073340]

Nel AXT, Madler L, Li N. Toxic potential of material at the nanolevel. Science. 2006; 311:622–627. [PubMed: 16456071]

Piao CQ, Liu L, Zhao YL, Balajee AS, Suzuki M, Hei TK. Immortalization of human small airway epithelial cells by ectopic expression of telomerase. Carcinogenesis. 2005; 26:725–731. [PubMed: 15677631]

Pirela S, Molina R, Watson C, Cohen JM, Bello D, Demokritou P, Brain J. Effects of copy center particles on the lungs: a toxicological characterization using a Balb/c mouse model. Inhalation Toxicology. 2013a; 25:498–508. [PubMed: 23895351]

Pirela S, Molina R, Watson C, Cohen JM, Bello D, Demokritou P, Brain J. Effects of copy center particles on the lungs: a toxicological characterization using a Balb/c mouse model. Inhal Toxicol. 2013b; 25:498–508. [PubMed: 23895351]

Pirela SV, Pyrgiotakis G, Bello D, Thomas T, Castranova V, Demokritou P. Development and characterization of an exposure platform suitable for physico-chemical, morphological and toxicological characterization of printer-emitted particles (PEPS). Inhalation Toxicology. 2014a

Pirela SV, Sotiriou GA, Bello D, Shafer M, Krumeich F, Bunker KL, Castranova V, Thomas T, Demokritou P. A case study of life-cycle implications from nano-enabled products: Consumer exposures to printer-emitted nanoparticles. 2014b

Rahal A, Kumar A, Singh V, Yadav B, Tiwari R, Chakraborty S, Dhama K. Oxidative Stress, Prooxidants, and Antioxidants: The Interplay. Biomed Res Int. 2014; 2014:761264. [PubMed: 24587990]

Roberts RA, Smith RA, Safe S, Szabo C, Tjalkens RB, Robertson FM. Toxicological and pathophysiological roles of reactive oxygen and nitrogen species. Toxicology. 2010; 276:85–94. [PubMed: 20643181]

Roy R, Kumar S, Tripathi A, Das M, Dwivedi PD. Interactive threats of nanoparticles to the biological system. Immunol Lett. 2014; 158:79–87. [PubMed: 24316409]

Scheller J, Garbers C, Rose-john S. Interleukin-6: From basic biology to selective blockade of pro-inflammatory activities. Semin Immunol. 2014; 26:2–12. [PubMed: 24325804]

Schripp T, Wensing M, Uhde E, Salthammer T, He C, Morawska L. Evaluation of ultrafine particle emissions from laser printers using emission test chambers. Environ Sci Technol. 2008; 42:4338–4343. [PubMed: 18605552]

Shao R, Guo X. Human microvascular endothelial cells immortalized with human telomerase catalytic protein: a model for the study of in vitro angiogenesis. Biochem Biophys Res Commun. 2004; 321:788–794. [PubMed: 15358096]

Slesinski RS, T D. Chronic Inhalation exposure of rats for up to 104 weeks to a non-carbon-based magnetite photocopying toner. Int J Toxicol. 2008; 27:427–439. [PubMed: 19482822]

Snyder-Talkington BN, Dymacek J, Porter DW, Wolfarth MG, Mercer RR, Pacurari M, Denvir J, Castranova V, Qian Y, Guo NL. System-based identification of toxicity pathways associated with multi-walled carbon nanotube-induced pathological responses. Toxicol Appl Pharmacol. 2013; 272:476–489. [PubMed: 23845593]

Snyder-Talkington BN, Q Y, Castranova V, Guo NL. New perspectives for in vitro risk assessment of multiwalled carbon nanotubes: application of coculture and bioinformatics. J Toxicol Environ Health B Crit Rev. 2012; 15:468–492. [PubMed: 23190270]

Snyder-Talkington BN, S-B D, Castranova V, Qian Y, Guo NL. Multi-walled carbon nanotubes induce human microvascular endothelial cellular effects in an alveolar-capillary co-culture with small airway epithelial cells. Particle and Fibre Toxicology. 2013

Sotiriou GA, Diaz E, Long MS, Godleski J, Brain J, Pratsinis SE, Demokritou P. A novel platform for pulmonary and cardiovascular toxicological characterization of inhaled engineered nanomaterials. Nanotoxicology. 2012; 6:680–690. [PubMed: 21809902]

Sriram K, Lin GX, Jefferson AM, Roberts JR, Andrews RN, Kashon ML, Antonini JM. Manganese accumulation in nail clippings as a biomarker of welding fume exposure and neurotoxicity. Toxicology. 2012; 291:73–82. [PubMed: 22085607]

Strieter RM, Mehrad B. New mechanisms of pulmonary fibrosis. Chest. 2009; 136:1364–1370. [PubMed: 19892675]

Szmitko PE, Wang CH, Weisel RD, De Almeida JR, Anderson TJ, Verma S. New markers of inflammation and endothelial cell activation: Part I. Circulation. 2003; 108:1917–1923. [PubMed: 14568885]

Tabima DM, Frizzell S, Gladwin MT. Reactive oxygen and nitrogen species in pulmonary hypertension. Free Radic Biol Med. 2012; 52:1970–1986. [PubMed: 22401856]

Volk T, Hensel M, Schuster H, Kox WJ. Secretion of MCP-1 and IL-6 by cytokine stimulated production of reactive oxygen species in endothelial cells. Mol Cell Biochem. 2000; 206:105–112. [PubMed: 10839200]

Wallace WA, Fitch PM, Simpson AJ, Howie SE. Inflammation-associated remodelling and fibrosis in the lung - a process and an end point. Int J Exp Pathol. 2007; 88:103–110. [PubMed: 17408453]

Wang H, He C, Morawska L, Mcgarry P, Johnson G. Ozone-initiated particle formation, particle aging, and precursors in a laser printer. Environ Sci Technol. 2012; 46:704–712. [PubMed: 22191732]

Watson C, Ge J, Cohen J, Pyrgiotakis G, Engelward BP, Demokritou P. High-throughput screening platform for engineered nanoparticle-mediated genotoxicity using CometChip technology. ACS Nano. 2014; 8:2118–2133. [PubMed: 24617523]

Wensing M, Schripp T, Uhde E, Salthammer T. Ultra-fine particles release from hardcopy devices: sources, real-room measurements and efficiency of filter accessories. Sci Total Environ. 2008; 407:418–427. [PubMed: 18809204]

Zeidler-erdely P, Battelli L, Salmen-muniz R, Li Z, Erdely A, Kashon M, Simeonova P, Antonini J. Lung tumor production and tissue metal distribution after exposure to manual metal ARC-stainless steel welding fume in A/J and C57BL/6J mice. J Toxicol Environ Health A. 2011; 74:728–736. [PubMed: 21480047]

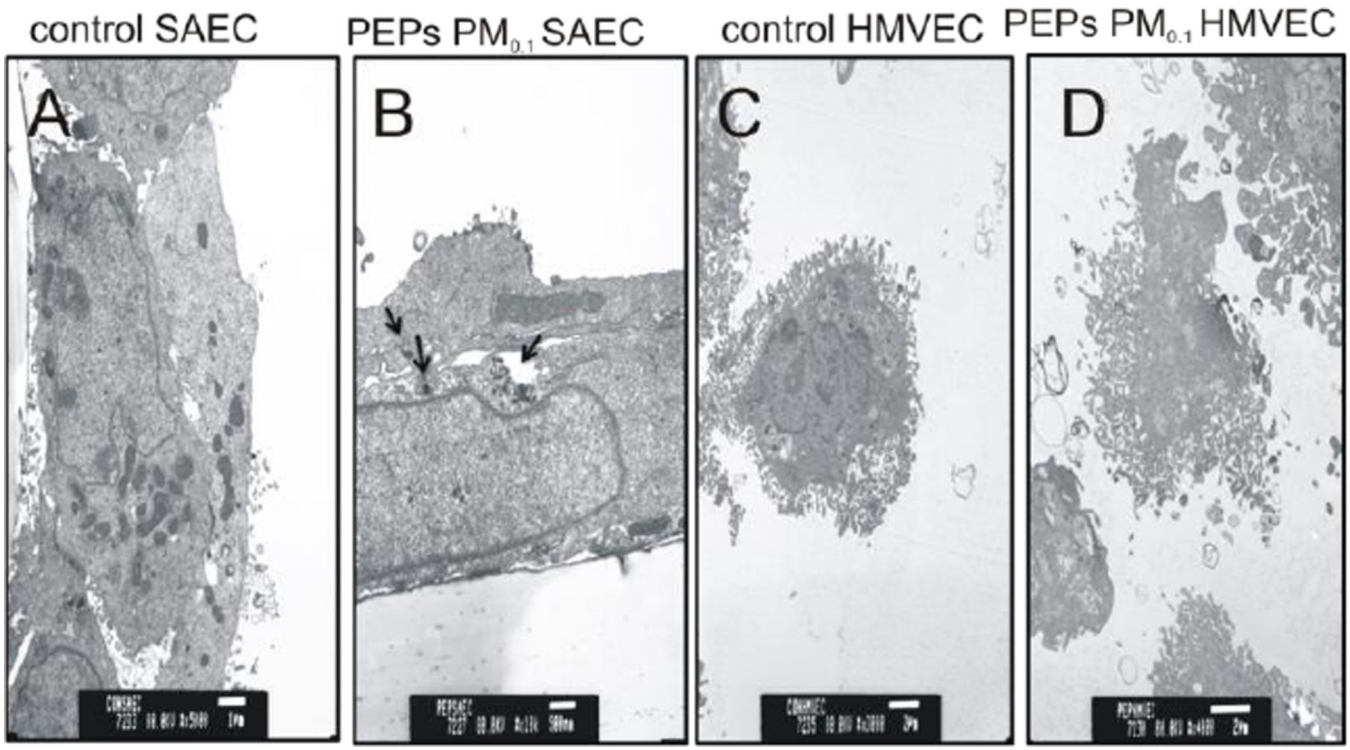

Figure 1. TEM images of SAEC and HMVEC after PEPs $PM_{0.1}$ exposure

SAEC were treated with 1.0 μg/mL PEPs $PM_{0.1}$ in the co-culture model for 24 h. Both SAEC and HMVEC were fixed with Karnovsky's fixative, stained with osmium and imaged with a transmission electron microscope. (A) SAEC treated with dIH_2O. (B) SAEC treated with PEPs $PM_{0.1}$, particles are identified with arrows. (C) HMVEC from the basolateral chamber after SAEC treatment with dIH_2O. (D) HMVEC from the basolateral chamber after SAEC treatment with PEPs $PM_{0.1}$. Images represent n = 3.

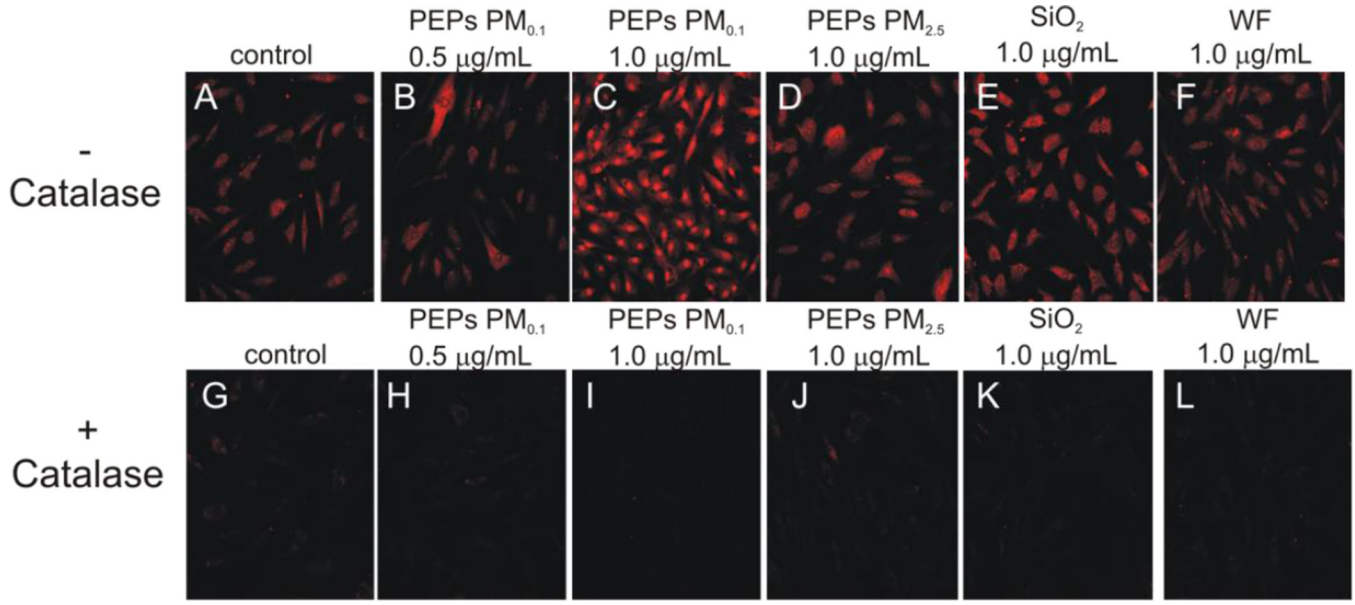

Figure 2. Reactive oxygen species are increased in HMVEC when SAEC are treated with PEPs

HMVEC were treated with 5 μM DHE for the last 30 min of 24 h treatment of SAEC with (A) control, (B) PEPs $PM_{0.1}$ 0.5 μg/mL, (C) PEPs $PM_{0.1}$ 1.0 μg/mL, (D) PEPs $PM_{2.5}$ 1.0 μg/mL, (E) SiO_2 1.0 μg/mL, and (F) WF 1.0 μg/mL. (G-L) HMVEC were pre-treated with 2000 U/mL catalase for 1 h. Images were taken using a Zeiss LSM510 microscope. Images are a representation of n = 3.

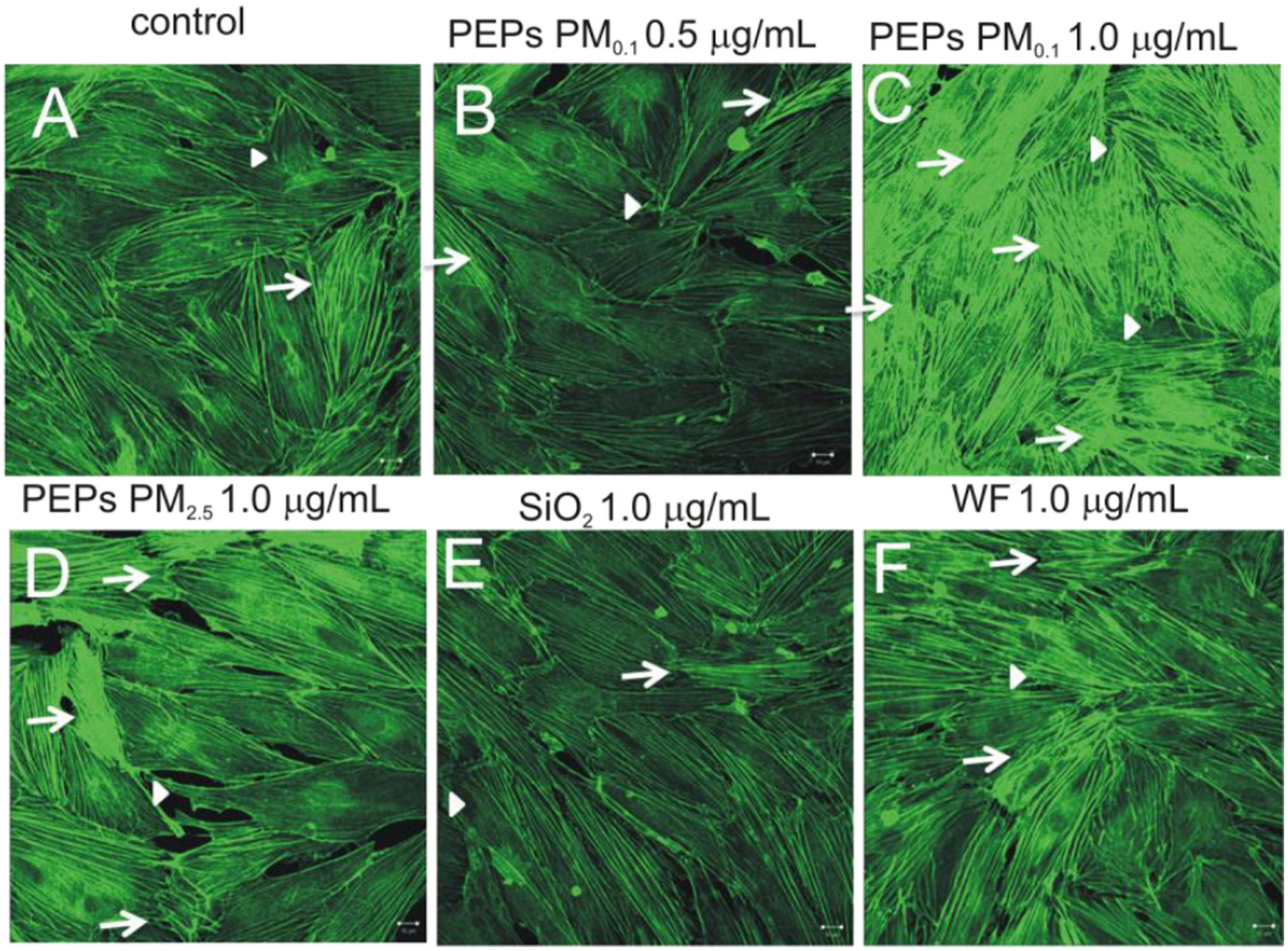

Figure 3. SAEC exposure to PEPs increases actin filament remodeling in HMVEC

HMVEC were grown on coverslips in the co-culture model and stained with AlexaFluor 546. (A) Control, (B) PEPs $PM_{0.1}$ 0.5 μg/mL, (C) PEPs $PM_{0.1}$ 1.0 μg/mL, (D) PEPs $PM_{2.5}$ 1.0 μg/mL, (E) SiO_2 1.0 μg/mL, and (F) WF 1.0 μg/mL. Arrows represent increase actin-filament stress fibers and arrowheads indicate increase filopodia and lamellipodia. Images were taken using a Zeiss LSM510 microscope. Images are a presentation of n = 3.

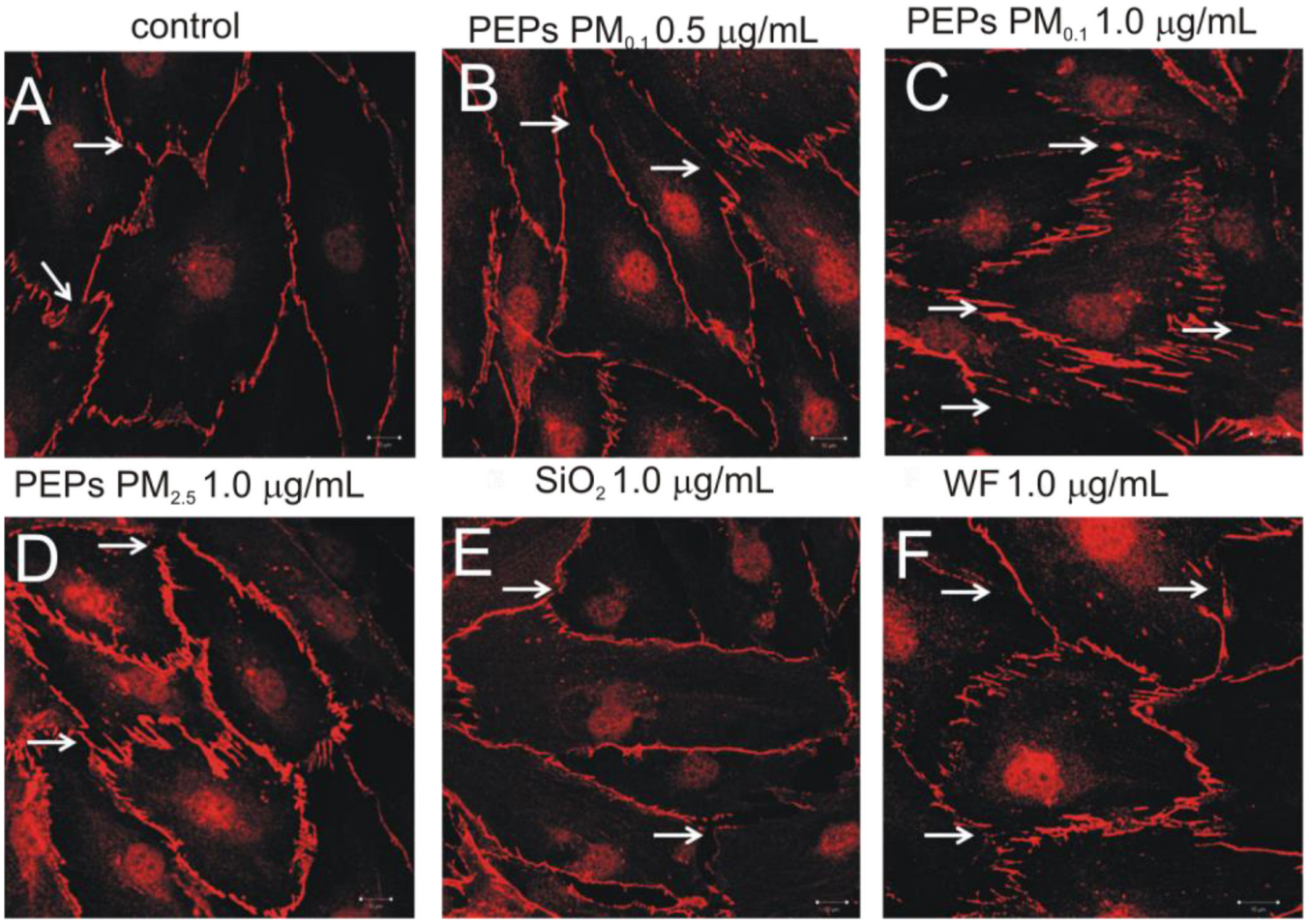

Figure 4. SAEC exposure to PEPs causes an increase in gap formations in the endothelial monolayer

HMVEC were grown on coverslips in the co-culture model, stained with rabbit anti-VE Cadherin and secondary anti-rabbit Alexa Fluor 647. (A) Control, (B) PEPs $PM_{0.1}$ 0.5 µg/mL, (C) PEPs $PM_{0.1}$ 1.0 µg/mL, (D) PEPs $PM_{2.5}$ 1.0 µg/mL, (E) SiO_2 1.0 µg/mL, and (F) WF 1.0 µg/mL. Arrows indicate gap formation with the endothelial monolayer. Images were taken using a Zeiss LSM510 microscope. Images are a presentation of n = 3.

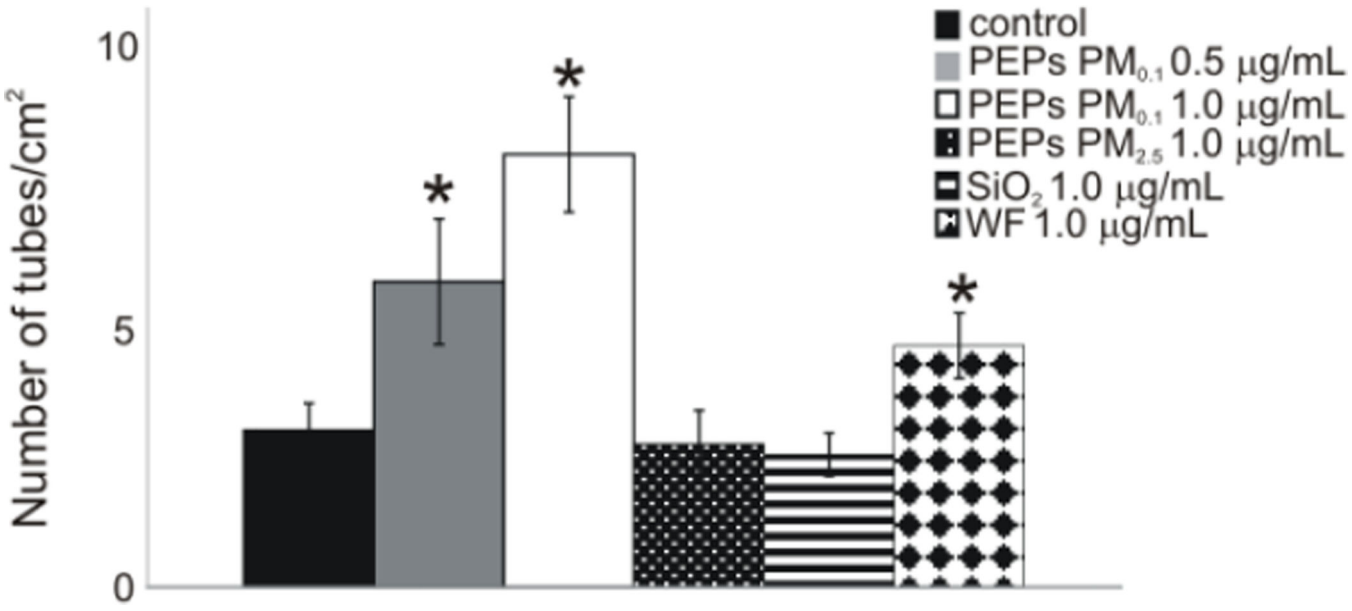

Figure 5. HMVEC exhibit increased angiogenesis due to SAEC treatment with PEPs

The quantification of the tube formation in HMVEC within the various treatments at 10× magnification. Pictures are a representation of n =3. * indicates $p < 0.05$ compared to control.

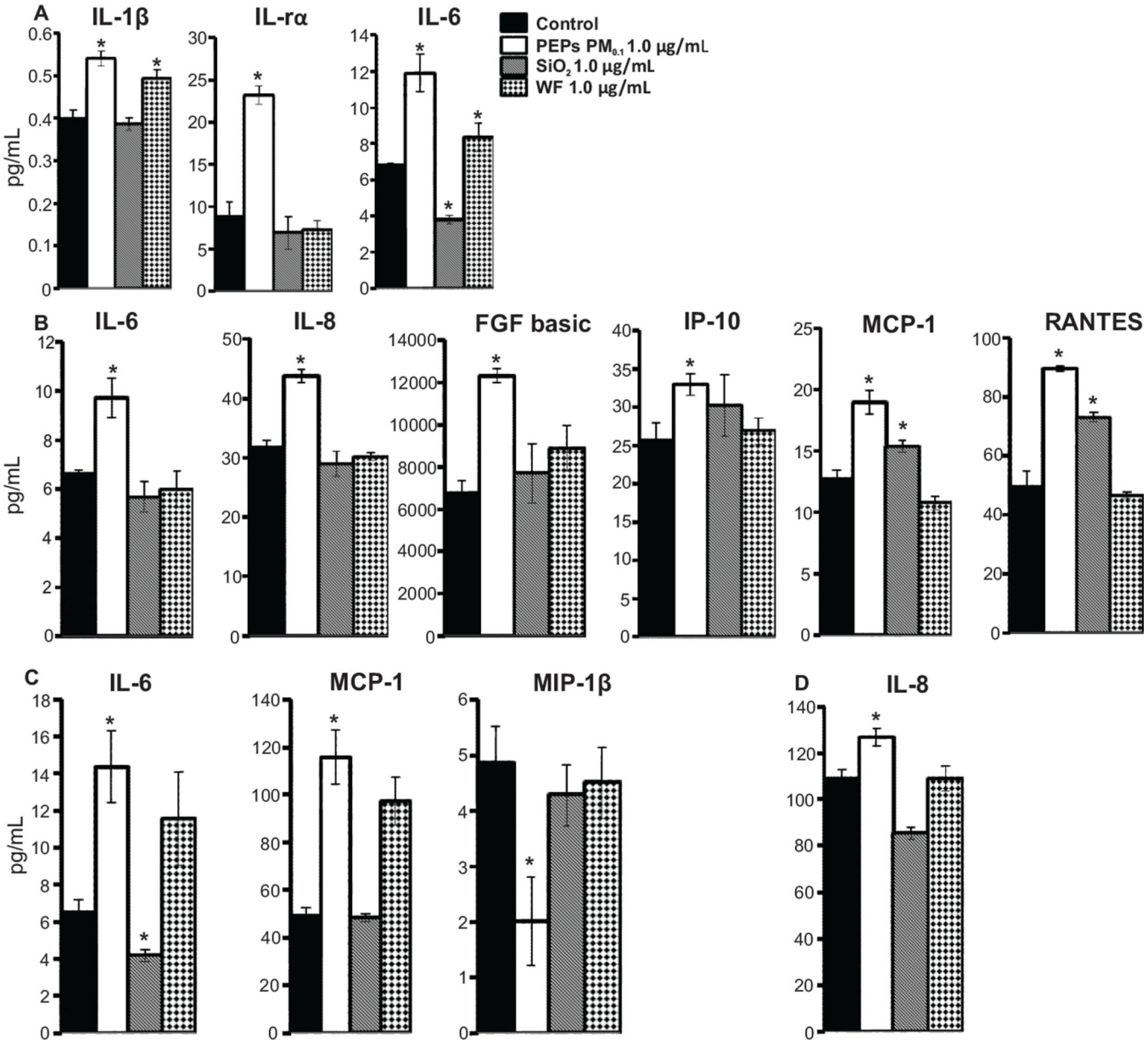

Figure 6. Cytokine and chemokine analysis

(A) IL-1b, IL-1ra, IL-6 levels were measured in SAEC condition media, (B) IL-6, IL-8, FGF basic, IP-10, MCP-1 and RANTES are shown in the cellular lysates of SAEC, (C) IL-6, MCP-1, and MIP-1b are shown within the condition media of HMVEC, (D) IL-8 shown in the cellular lysates. Cytokines and chemokines were analyzed after a 24 h treatment of SAEC with PEPs $PM_{0.1}$ 1.0 μg/mL, and SiO_2 1.0 μg/mL and WF 1.0 μg/mL. n = 3, * indicates $p < 0.05$ compared to control.

Table 1

Properties of ENMs dispersions in dIH_2O and SABM.

Nanomaterial	Media	dH (nm)	PdI	ζ (mV)	σ (mS / cm)	Effective Density (g/cm^3)
PEPs $PM_{0.1}$	**dIH_2O**	178.3 ± 3.5	0.403 ± 0.05	−20.6 ± 1.9	0.185 ± 0	
	SABM pH 7.4	381.7 ± 40.2	0.586 ± 0.05	9.97 ± 2.8	2.52 ± 0.0721	2.39
PEPs $PM_{2.5}$	**dIH_2O**	197.8 ± 17.4	0.441 ± 0.06	−16.0 ± 1.01	0.351 ± 0	
	SABM pH 7.4	231.1 ± 2.9	0.348 ± 0.005	−17.7 ± 3.6	3.61 ± 0.590	3.10
SiO_2	**dIH_2O**	142.5±2.4	0.207±0.01	33.6±1.70	0.00804±0	
	SABM pH 7.4	663.8 ± 124.5	0.277 ± 0.09	28.4 ± 6.0	10.5 ± 0	1.20
WF	**dIH_2O**	2197 ± 118.4	0.561 ± 0.4	8.52 ± 1.2	0.0284 ± 0	
	SABM pH 7.4	1526.7 ± 259.6	0.198 ± 0.04	18.8 ± 0.9	10.5 ± 0.462	1.37

d_H: hydrodynamic diameter, PdI: polydispersity index, ζ: zeta potential, σ: specific conductance.

Note: Values represent the mean (± SD) of a triplicate reading. Footnote: the average diameters obtained from DLS characterization are derived from the intensity-weighted distributions based on the intensity of light scattered by the particle.